Materials Transactions, Vol. 60, No. 7 (2019) pp. 1243 to 1255
Special Issue on Severe Plastic Deformation for Nanomaterials with Advanced Functionality

Corrosion Behavior of Severely Deformed Pure and Single-Phase Materials

Hiroyuki Miyamoto[1], Motohiro Yuasa[1], Muhammad Rifai[2] and Hiroshi Fujiwara[3]

[1]*Department of Mechanical Engineering, Doshisha University, Kyotanabe 640-0394, Japan*
[2]*Center for Science and Technology of Advanced Materials, National Nuclear Energy Agency, Batan, Indonesia*
[3]*Department of Mechanical Engineering, Shizuoka Institute of Science and Technology, Shizuoka 437-8555, Japan*

The significant and complex effect of plastic deformation on corrosion behavior involves changes in not only dislocation density but also other metallurgical factors such as grain size, texture, chemical inhomogeneity, phase transformation and residual stress. With the advent of severe plastic deformation (SPD), the effect of plastic deformation on corrosion in the ultrahigh strain range is becoming an important issue. However, our understanding of corrosion properties of SPD materials lags far behind than that of their other properties, e.g. their mechanical properties. In this review, the role of dislocations and grain boundaries generated by SPD was highlighted in pure metals and single-phase materials, where plastic deformation and grain refinement proceed mainly by dislocation activity. Accordingly, the complicated effect of chemical inhomogeneity arising from impurity segregation and precipitation was excluded from discussion, while other implicit effects were included. It is essential to elucidate the effect of so-called ultrafine-grained (UFG) structures which develop progressively to a saturation over a very wide strain range. Unfortunately, the literature mainly compares the corrosion behavior of UFG and coarse-grained (CG) materials, and the degree of perfection of UFG formation and the resultant effects on corrosion vary between studies. The limited number of studies that examines corrosion behavior systematically over a wide strain range suggests that, in most cases, the effect of plastic deformation on corrosion extends into the SPD region gradually, with no anomalous change. That is, SPD improves the corrosion resistance to further degree in a passive environment, whereas it increases the dissolution rate in a non-passive environment. However, several works reported an abrupt change in corrosion resistance, which could be attributed to UFG formation. A marked improvement is observed in Fe–Cr alloys, where passivation becomes more protective owing to UFG formation induced by SPD. In severely deformed materials, structural alterations in dislocations and grain boundaries have a very high impact on the corrosion kinetics because of their closely spaced configuration. [doi:10.2320/matertrans.MF201935]

(Received February 25, 2019; Accepted April 1, 2019; Published June 7, 2019)

Keywords: *corrosion, severe plastic deformation (SPD), ultrafine-grained (UFG) structures, dislocation, grain boundary*

1. Introduction

The fabrication of metallic materials for load-bearing structural components often involves plastic deformation process, such as rolling, forging, and pressing. Therefore, the effect of plastic deformation on the corrosion properties as well as mechanical properties of these metallic materials has become an issue of great practical concern.[1–7] Plastic deformation generates various crystal defects such as dislocations, grain boundaries, vacancies, and twins. Thermodynamically, the internal energy stored as these crystal defects enhances the driving force of an electrochemical reaction by lowering the electrode potential of the anodic reaction. However, the impact of that stored energy on corrosion is not as strong as the impact of alteration in chemical inhomogeneity arising from impurity and alloying elements as a result of plastic deformation.[7]

With the advent of severe plastic deformation (SPD) represented by equal-channel angular pressing (ECAP),[8] high-pressure torsion (HPT),[9] accumulative roll bonding (ARB)[10] as a new process for fabricating bulk nanocrystalline (NC) or ultrafine grained (UFG) materials, the effect of plastic deformation on corrosion has once again become a very important topic. The magnitude of plastic strain in SPD is much higher than that in conventional processes, with equivalent plastic strain values ranging from about 4 to over 20–30.[11–13] That corresponds to a maximum dislocation density of nearly $10^{15}\,m^{-2}$ in pure copper[14–16] and the final grain size is reduced to 0.4 μm by ECAP at room temperature,[17,18] and 80 nm by HPT at 100 K.[19] Such high density defects may impact corrosion behavior even in pure metals or single-phase materials. Indeed, increasing number of works show large changes in corrosion behavior due to SPD (e.g., see Refs. 20, 21). Fortunately, for most materials, corrosion resistance is improved by SPD in passivation-forming environments although there are some contradictory reports for the same materials and the same environment.[20] The reason of the seeming contradiction or discrepancy is unknown, but small difference in phase composition, impurity content or residual stress have been suspected.[20]

Despite the complicated effects of SPD on corrosion, many attempts have been made to find a general rule of corrosion behavior, and in most cases, grain size is regarded as a key parameter governing corrosion resistance.[21–29] Ralston *et al.* reported that in terms of corrosion resistance, UFG/NC materials are superior (inferior) to coarse-grained (CG) materials in passive (non-passive) environments.[21] This is mainly because grain boundaries have high energy and are reactive to solutions, therefore they enhance the kinetics of both passivation and anodic dissolution. Ralston *et al.* also proposed a Hall-Petch type relationship between corrosion current and grain size that can be applied to pure aluminum and magnesium within a reasonable margin of error.[25]

In severely deformed materials, which typically show strains higher than 4, a UFG structure having a high density of deformation-induced grain boundaries with high misorientation angle develops. These grain boundaries are considered to be at a non-equilibrium state, with extra grain boundary energy due to extrinsic grain boundary dislocations.[30,31] For detail on non-equilibrium grain boundaries, please see the recent review by Nazarov.[32] Non-equilibrium grain boundaries, or alternatively grain boundaries of non-equilibrium configuration,[33] may impact the corrosion behavior of severely deformed materials. Indeed, there are cases in which corrosion behavior of SPD materials cannot be predicted by extrapolating from the conventional processing

regime where the microstructure typically consists of dislocation substructures.[29,34–36] Similarly, corrosion behavior is altered by post-SPD flush annealing, which results in little change in grain size and microstructure.[37–43] These anomalous changes in corrosion behavior with increasing strain due to SPD and post-SPD annealing with insignificant grain size change are attributable to the high density of non-equilibrium grain boundaries and/or residual dislocations. In the ultrahigh strain range, microstructural features like dislocation density, misorientation and structures of grain boundaries, develop progressively into an ultimate form of UFG with variation in flow stress, stored energy, and grain size.[16] Thus, it is of interest to know how the gradual transition from dislocation structures to UFG affect the corrosion behavior. The seeming contradiction or discrepancy in the literature as to the impact of SPD on corrosion behavior may be attributed to the differences in the level of perfection of the UFG structures. This was the main motivation behind the present review. If true, not only the amount of the energy stored as these lattice defects, but also their configuration and distribution would affect the kinetics of corrosion.[5] Dislocations and grain boundaries locally have high stored energy, and they can form galvanic couples with the surrounding perfect crystals.[44,45] The nanoscale potential distribution has recently been determined by a Kelvin probe force microscopy,[46,47] scanning Kelvin probe microscopy (SKEM),[48] nanoscale galvanic cells between grain boundaries and dislocations with the surrounding matrix have been revealed by in situ observation using electrochemical scanning tunneling microscopy (ECSTM),[49–51] scanning transmission electron microscopy (STEM),[52] and open-loop electric potential microscopy (OL-EPM).[53,54] These experimental results validate the hypothesis that nonuniformity of electron activity is maintained to nanoscale structures with sufficient potential difference to form galvanic cells. This indicates that when the density of dislocations or grain boundaries becomes extremely high, the effect of their structures on corrosion can be appreciably high due to the closely spaced configuration. This was the second motivation. In this review, the corrosion behavior of severely deformed materials is surveyed to provide an overview of the literature on the effect of the UFG structure on corrosion in order to organize the relevant studies into a coherent whole in the simple materials.

Plastic deformation also affects corrosion behavior through other effects such as alteration of the solute element distribution,[55,56] the partial or complete dissolution of precipitates[57] and their physical fragmentation,[57–69] phase transformation,[70,71] texture change,[37,72–75] and residual stress enhancement.[41,73,74,76,77] We limit ourselves to simple materials, such as pure metals and single-phase alloys so that we can neglect the very complex effect of chemical inhomogeneity, and rather focus on the effect of the evolution of deformation-induced microstructures in severely deformed materials.

2. Microstructure of Deformed and Severely Deformed Materials

The deformation structures develop, through several stages, from dislocation substructures at an early stage into UFG microstructures with a high density of deformation-induced grain boundaries at the ultrahigh strain. The crystal structure and stacking fault energy (SFE) of materials play critical roles in determining their deformation modes and thus the SPD-induced grain refinement mechanism.[78,79] The mechanism of UFG formation has been described elsewhere,[78,80,81] and not described here. This paper focus on the distribution of major defects, i.e., dislocations and deformation-induced grain boundaries developed in FCC metals with medium to high SFE materials, and BCC and HCP materials where plastic deformation and grain refinement proceed via dislocation activity. In FCC metals with low SFE, and BCC and HCP under a special deformation condition such as high strain rate and/or low temperature (in the regime of very high Zener-Hollomon parameter), the deformation and UFG formation mechanisms change dramatically from mechanisms involving dislocations activity to mechanism involving deformation twinning.[78] The corrosion behavior of these latter materials is included here only briefly, although the topic is of practical importance. Magnesium and its alloys are special in that they are processed at moderately high homologous temperature of 200 to 300°C, so that the grain size is relatively large and frequently inhomogeneous because of dynamic recrystallization.[24,39]

Figure 1 illustrates the microstructural evolution of deformed FCC materials with medium to high SFE. BCC and HCP materials deformed under a low Z-H parameter deforms by the similar mode, and can be included in this mode of deformation. In early stage 1 (1 to 4 passes in copper as shown in Fig. 2), rapid dislocation accumulation occurs with the formation of cell walls, and there are many diffuse small angle boundaries. In stage 2 (4–12 passes in Fig. 2), the dislocations density starts to decrease by forming high-angle grain boundaries and correspondingly the fraction of high angle boundaries increases rapidly. In stage 3 (12– passes in

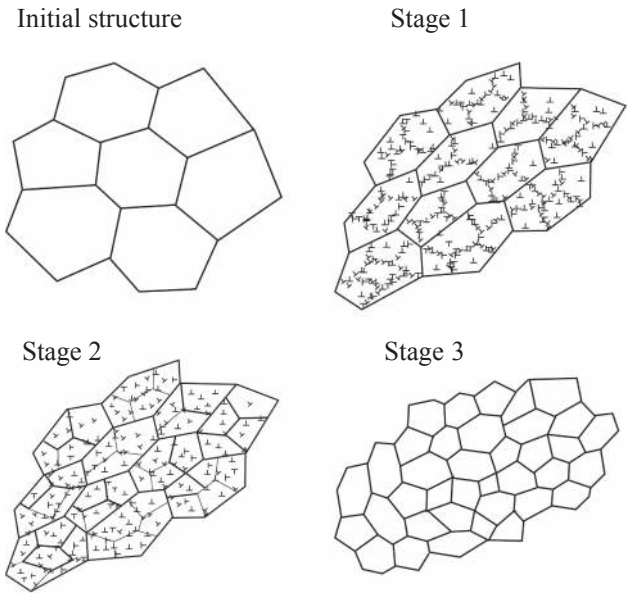

Fig. 1 Schematic diagram showing progressive development of dislocations structures and grain refinement mechanism where dislocations slip play a primary role.[78]

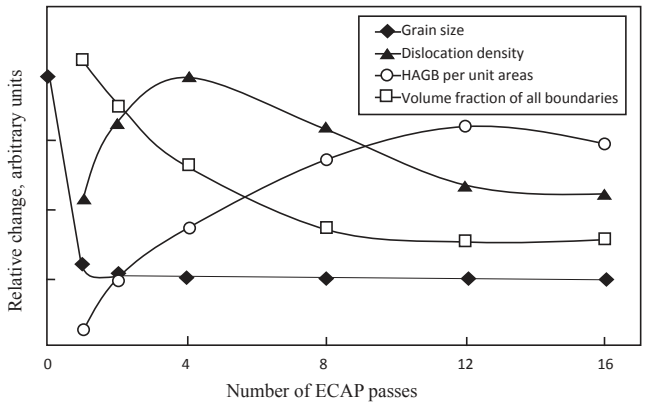

Fig. 2 Progressive changes of grain size, dislocation density, density of high-angle grain boundaries and volume fraction all boundaries in pure copper.[82)]

Fig. 2), microstructures comprising equiaxed UFGs evolves as the ultimate form. At this stage, the grain size is typically smaller than 1 μm with predominantly HAGBs and very few residual dislocations inside grains as revealed by transmission electron microscopy (TEM). This can be regarded as the *ideal* UFG structure, the typical microstructure of *severely deformed* materials, as distinct from that of *deformed* materials. Figure 2 shows the variation of relative change of fraction or density of defects.[82)] The transition from stage 2 to 3 is gradual, and the grain size and the minimum plastic strain required to attain *ideal* UFG structure is not known but depend on materials,[79)] deformation route[83,84)] and hydraulic pressure.[85)] In general, materials with low melting temperatures and/or high SFE such as pure aluminum tend to attain the *ideal* UFG structure under a lower plastic strain but reach to *saturation* at a large grain size.[86)] After the stage 2, grain size becomes essentially constant as shown in Fig. 2. Therefore, it can be difficult to determine the degree of maturity of UFG structure by bright-field TEM; that often requires a detailed examination of residual dislocations by high-resolution TEM and quantitative observation of the misorientation of grain boundaries by electron-back scattered diffraction (EBSD).[87)]

An important feature of SPD materials is the dislocation-induced grain boundaries, regarded as non-equilibrium grain boundaries with extra grain dislocations (extrinsic dislocations).[30,31)] Such non-equilibrium grain boundaries, also referred to grain boundaries with non-equilibrium configuration,[33)] are a characteristic component of UFG materials fabricated by SPD. The energy of non-equilibrium grain boundaries of copper with a grain size of 0.2 μm was estimated to be 1.2 J/m^2,[88)] which is almost twice that of recrystallized materials. Therefore, they could be more susceptible to local attack in aggressive media than equilibrium grain boundaries,[20)] and they have more or less impact on the corrosion resistance of UFG materials. It should be noted that such non-equilibrium grain boundaries exert a high internal stress inside grains near the grain boundaries.[89)] The internal strain of grains, calculated on the basis of the spreading of thickness extinction contours, was found to reach to 3×10^{-3} near grain boundaries of pure copper with a grain size of 0.2 μm.[89,90)] Similarly, X-ray diffraction studies revealed that the internal strain in UFG Cu processed by ECAP is about 10^{-3}–10^{-4}. This internal stress or strain is elastic in nature, and while it may increase the internal energy, it lowers the kinetics of the anodic reaction if it is compressive.[45)] The effect of that internal stress on corrosion behavior has been discussed in the literature.[34,39,91–94)] However, it seems that this internal stress is often confused with the classic residual stress;[60,93–95)] the former is considered to be local and associated with grain boundary structures while the latter is more of a macro stress arising from a non-uniform deformation or thermal history. Thus, the effect of the local internal stress near the grain boundaries are quite complex, which is often superimposed with the residual stress, and it waits future investigations.

The most notable properties of non-equilibrium grain boundaries are their fast diffusion kinetics.[96–100)] This kind of rapid diffusion would be expected to impact the materials properties, especially time-dependent properties like creep and the corrosion behavior. Ultrafast diffusion of Cr in nanocrystalline Fe processed by SMAT was reported,[100)] and this may be the cause of enhanced corrosion resistance of Fe–Cr alloys.[29)] Non-equilibrium grain boundaries are not stable, and they can be recovered to an equilibrium state by post-SPD annealing at a mild temperature.[33,101,102)] For pure copper, an X-ray study revealed that the internal strain was completely recovered at post-SPD annealing at 423 K for 30 minutes with little grain growth.[101)] For high purity copper (99.9999%), it is shown that the internal strain will diminish even at room temperature after six hours.[103)]

During plastic deformation, the internal energy is stored in the form of lattice defects such as dislocations, grain boundaries, vacancies, twins, etc.,[16,104,105)] and it is the basic property affecting the stability of many materials' physical and chemical behavior including their corrosion behavior. During SPD, the stored energy increases rapidly in the early stages of strain, which is indicative of the dislocation accumulation, then increases gradually, saturating at an extremely high plastic strain.[16,104,105)] Figure 3 shows the variation of total grain boundary energy and energy stored as dislocations in pure copper pressed by ECAP.[16)] The boundary energy of pure copper increased rapidly to about 0.3 J/g after 2 passes, and then increased at a very slow rate to a saturation value upon further ECAP passes.[16)] On the other hand, total dislocation energy increased up to 5 passes, reflecting increasing dislocation density shown in Fig. 2, and

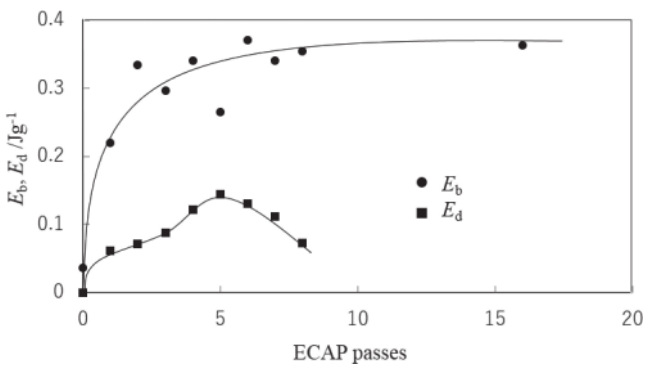

Fig. 3 Variation of stored energy of grain boundaries, E_b and dislocations E_d as a function of ECAP passes.[16)]

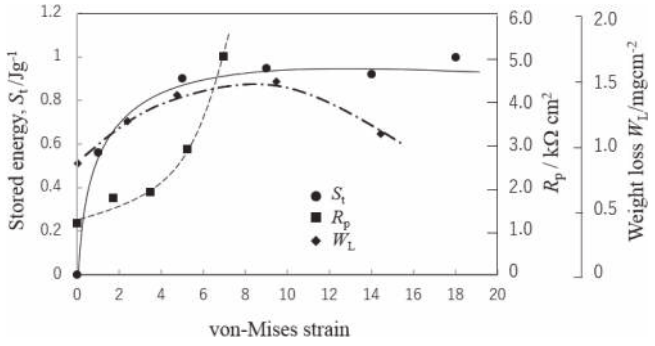

Fig. 4 Variation of total stored energy,[104] resistance, passive film resistance Rp,[34] and weight loss in immersion test in Livingston's dislocation etchant[110] of pure copper with increasing strain.

decreased thereafter owing to the absorption at grain boundaries. Since the total stored energy is almost constant as shown later in Fig. 4, the decrease in the dislocation energy is mostly compensated by energy stored as grain boundary energy, while some of it is transformed to the additional energy of non-equilibrium grain boundaries. It is reported that a rather large fraction of the energy is stored as vacancies,[106] whose concentration can exceed 2.0×10^{-4}, which is comparable to the levels observed close to the melting temperatures of these materials. Since the stored energy as a thermodynamic variable, which cause a possible shift of electrode potential in a more active direction, the first step is to survey the literature on the possible effect of the stored energy on corrosion behavior over a wide range of plastic strain. Unfortunately, there are limited studies which examines the corrosion behavior over a wide range of plastic strain. Nevertheless, several studies present the corrosion trends over a wide strain range from conventional up to SPD values.[34,36,39,58,95,107–114] Some of these studies report an anomalous change in corrosion behavior[34,36,95,110,113] and suggest the possible role of UFG structures on corrosion kinetics, as described later.[36]

3. Corrosion Studies of Severely Deformed Metals

3.1 Past corrosion studies of SPD materials

The overall trends in the corrosion of, mostly, aluminum and magnesium with grain size reduction have been reviewed by Ralston *et al.*,[21] and the trends for a wider range of materials with a greater emphasis on the different types of SPD have been reviewed by the present author.[20] For pure metals, Ralston *et al.* proposed the general rule that UFG and NC materials exhibit a higher corrosion rate than CG materials in non-passivating environments.[21] In their review, they employ a Hall-Petch type law to correlate within a reasonable error, the corrosion resistance of materials processed by various methods including SPD with the grain size as a common metallurgical variable.[21]

ECAP is the most common SPD method used in almost half of the studies on corrosion of severely deformed materials.[20] Other traditional SPDs methods such as HPT,[115] ARB,[34,107] hydrostatic extrusion (HE),[67] and modified cold rolling[37] are also employed, albeit not as frequently. Corrosion is a surface phenomenon, thus so-called surface nanocrystallization (SNC) methods such as shot-blast/peening,[116–120] ultrasonic peening,[73,74,77,121] surface mechanical attrition treatment (SMAT),[24,27,56,122] and friction stir processing (FSP)[123] are also reported, and, in some cases, demonstrated as an effective approach in enhancing corrosion resistance.

3.2 Pure aluminum

In most corrosion studies of pure aluminum, the material was processed by ECAP.[59,68,108,124–128] The impact of SPD on corrosion resistance is much higher for pure aluminum than for other pure metals and it is mostly a favorable impact[27,58,59,68,91,124,127,128] with some exceptions.[57,107,108,125] The corrosion behavior is mainly characterized through polarization tests in neutral NaCl solutions aimed at determining the corrosion resistance on the basis of the corrosion current and pitting potential. In most cases, the corrosion current decreases[68,93,95,114] and the pitting potential increases[68,93] as compared with the values for CG materials. The anodic current is mostly suppressed by SPD, while the cathodic current is less affected near the open potential, suggesting that the spontaneous passive film become more protective upon UFG formation because of high-density grain boundaries which facilitate passivation.

The imposed strain or the number of ECAP passes vary between studies ranging from 4 to 8 passes.[57–60] Since pure aluminum has a high SFE and relatively low melting temperature, it becomes a complete UFG structure at relatively low plastic strain. However, there is still concern that the level of UFG reached differs from study to study, because corrosion properties do not saturate in the investigated strain range.[58,107,125] For example, corrosion currents continue to decrease and do not saturate until 9 ARB passes, which corresponds to an equivalent strain of 7.[95] Similarly, the pitting potential of commercial pure aluminum (A1050) continues to increase until the final 5 ECAP passes, do not show saturation.[58] On the other hand, Song *et al.* pressed commercial pure aluminum for up to 16 passes, and observed saturation with considerable improvement in pitting corrosion potential and suppression of corrosion current.[68,93] Therefore, the level of UFG formation attained by ECAP varies between studies, and the effect of UFG materials may be underestimated in these studies. Unfavorable effects by SPD are mainly attributed to small cathode precipitates which fragmented into even smaller pieces during SPD.[57,107,108,125] The degradation of corrosion resistance reported for nanostructured aluminum processed by surface mechanical attrition treatment (SMAT) has been attributed to high surface roughness.[27]

3.3 Pure magnesium

Although pure magnesium and its alloys are the second-best materials studied in this field, they are special in that they are processed by SPD at moderately higher homologous temperatures of 200 to 300°C because magnesium is difficult to deform due to its HCP structure.[24,28,39] Therefore, grain fragmentation involves continuous dynamic recrystallization, and reach to a saturation of microstructure by lower plastic strain. The final grain size and residual dislocation density are strongly affected by the initial grain size and deformation conditions such as the strain rate and temperature.[129]

Because of dynamic recrystallization, the microstructures tend to become inhomogeneous, or a bimodal mixture with coarse grains and UFG structures,[129] which may be one reason for the inconsistent results reported in the literature. Similarly, due to the enhanced recovery process, dislocations densities are relatively low and grain boundaries are in the equilibrium state. Thus, corrosion behavior is dominated by the inhomogeneous microstructure rather than the level of UFG and non-equilibrium grain boundaries. Corrosion properties of pure magnesium were examined using NaCl solutions[130] or artificial human body fluid,[129] and like pure aluminum, pure magnesium is mostly improved by SPD,[24,109,129–131] but with some exceptions.[39] It is evident that the very high fraction of grain boundaries is likely to reduce corrosion rates by accelerating the passivation kinetics, making the unstable passivation more protective. Similar to that of aluminum, the corrosion behavior of magnesium is sensitive to cathode precipitations, which greatly complicate the effect of SPD on corrosion in magnesium alloys, especially in low-impurity materials. In contrast with pure aluminum, effect of microstructural evolution on corrosion current is reflected in the decrease (or increase) of cathode reaction.[28,39,132,133] The reason of the suppression or promotion of cathode current due to UFG formation is unknown, but may be attributed to an enhanced kinetics of cathode reaction or electroconductivity of the passivation films.

3.4 Pure titanium

Thermodynamically, pure titanium is passive in solutions over the entire pH range and has very high corrosion resistance. UFG materials have been pressed by ECAP,[23,75,134–138] but other SPD methods such as HPT,[115] hydrostatic extrusion,[76,139] FSP,[123] and high-ratio differential speed rolling (HRDSR)[37,41] have also been employed. Like pure magnesium, pure titanium is difficult to deform at room temperature due to its HCP structure. Therefore, it is typically processed by SPD at relatively high temperatures such as 200°C[137] or 350 to 600°C.[23,75,76,134–136,138] except for HPT, which is usually done at room temperature.[115] Despite the higher SPD temperatures, the final grain size is small, typically on the order of 0.2 μm, and residual dislocations can be observed in most cases, suggesting immature UFG formation.[139] Corrosion of pure titanium has been studied for potential use in biomaterials, and like magnesium, they are in many cases evaluated in dilute 0.9% NaCl solution[76,136] or artificial body fluid.[23,135,137,138] with some exception using acidic solutions.[37,41] In most cases, as in other materials, corrosion resistance is evaluated by polarization tests and improved by SPD, although the degree of impact is smallest among the materials studied. Similar to pure aluminum, suppression of corrosion current is mainly dominated by anodic current near the open potential, and the passive current density is decreased.[23,137,139] Like other materials, this improvement of resistance to dissolution can be explained by the presence of a dense protective passive film due to accelerated passivation reaction in UFG materials. Inconsistent results have been reported for HPT, in which pure titanium was pressed to reduce the grain size to a surprising 100 nm and corrosion resistance was degraded.[115] The reason for this degradation is unknown, but high internal stress or phase transformation (α to ω) are possible causes. Unfortunately, there has been few work examining the corrosion behavior with a systematic increase of plastic strain,[136] and the majority of prior works have compared two microstructures of CG and UFG.[23,37,75,76,134,135,137,139] Sotniczuk *et al.*[139] reported that post-ECAP annealing improves corrosion resistance with little grain growth, and attributed this improvement to a reduction of residual dislocations. This interpretation suggests that the effect of SPD on corrosion becomes stronger with more pressing, achieving a more complete level of UFG formation with few dislocations inside the grains. Similarly, Kim *et al.*[41] and Gu *et al.*[75] also reported a positive effect of post-SPD annealing with little grain size change.

3.5 Pure copper

Pure copper has been employed in numerous studies for microstructural analysis after SPD using using TEM,[12,101,140,141] XRD,[106,142] EBSD.[17,143] It is a relatively noble material, and the effect of impurity segregation or cathode precipitation on corrosion is weak, so it is an ideal material to examine the effect of deformation microstructures on corrosion behavior. Thermodynamically, pure copper undergoes passivation in near-neutral and weak alkali regions, but the passivation layer is incomplete and less protective, and its growth is time-dependent. Therefore, pure copper at open potential in neutral solutions is naked upon immersion, but with time, it gets coated with passivation if the surface becomes reactive owing to the high density of dislocations and grain boundaries induced by SPD. Although the effect of severe deformation on the corrosion of pure copper is relatively weak compared with other materials, anomalous changes in corrosion behavior that may be attributed to UFG formation was observed. Figure 4 shows the variations in the polarization resistance, corrosion rate, and total stored energy upon plastic deformation of pure copper as a function of equivalent strain by SPD; the three data sets are from different sources.[34,104,110] The polarization resistance, R_p, of pure copper deformed by ARB was obtained by electrochemical impedance spectroscopy (EIS) in a 3.5% NaCl solution[34] and the corrosion rate of pure copper deformed by SSE was obtained by immersion tests in Livingston etchant.[110] The total internal energy, stored in lattice defects mainly as dislocations, grain boundaries and excessive vacancies by ECAP, is also plotted.[104] It is important to note that R_p, increases rapidly after 4 ARB passes despite the almost constant total stored energy. The increase in R_p, is attributed to the thicker and more protective passivation layer obtained with increasing number of ARB passes.[34] Similarly, the corrosion rate increases with increasing stored energy in Livingston's dislocation etchant, but it starts to decrease after 8 SSE passes, presumably upon the possible formation of a UFG structure.[110] In both cases, the change in corrosion behavior does not conform to the change in stored energy, suggesting that the transition to UFG may affect corrosion kinetics. Inversely, the corrosion rate of UFG copper increased by post-SPD annealing which results in little grain growth, possibly due to the recovery of UFG structures of as-ECAPed copper.[43,144] (In Ref. 43,

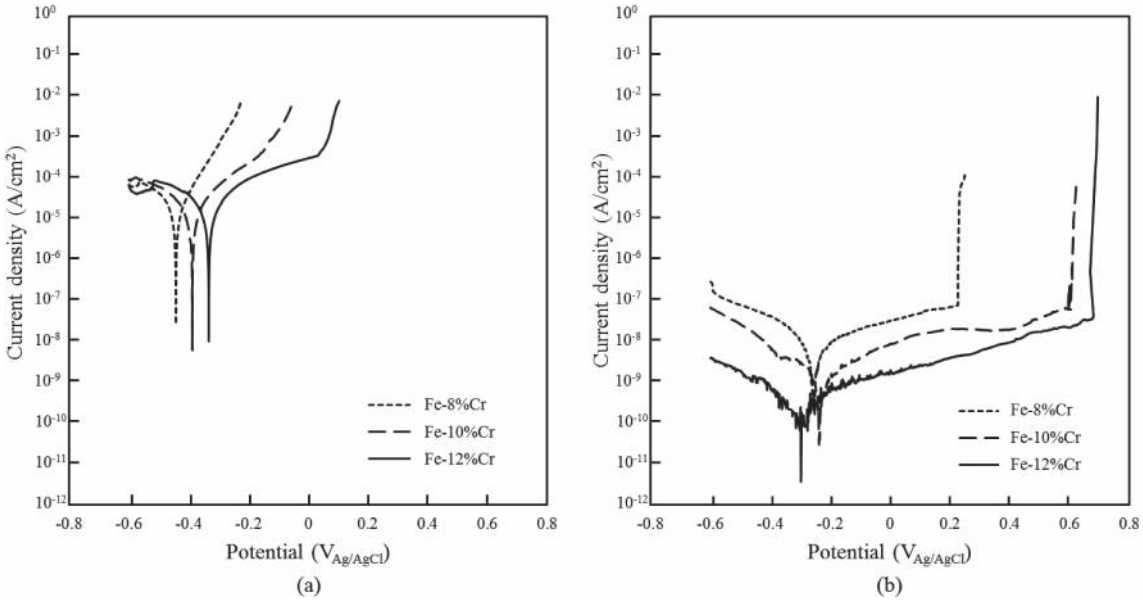

Fig. 5 Dynamic polarization curves of (a) CG, and (b) UFG Fe–8%, 10%, 12%Cr alloys in 3.5%NaCl solution.[35)]

the increase in corrosion rate was ascribed to an increasing fraction of HAGB although the grain size increased from 0.52 μm to 3.96 μm. In our opinion, the increase in corrosion rate was due to reduced protectiveness of the passivation by the lower dislocations and grain boundaries density, and possible recovery of non-equilibrium grain boundaries.)

3.6 Fe–Cr alloys

To the best of our knowledge, the corrosion resistance of Fe–Cr steels is enhanced by UFG formation without exception, and the degree of impact on corrosion resistance is highest among the materials investigated. We found that UFG Fe–20%Cr alloy fabricated by ECAP exhibited higher pitting potential than CG counterparts.[29)] This high pitting potential was partially reduced by post-ECAP annealing at 200°C for 3 minutes, which induced little grain growth.[29)] Therefore, we concluded that the high pitting potential was attributed to non-equilibrium grain boundaries, which facilitate protective passivity, and the partial degradation of corrosion resistance by post-SPD annealing was due to the recovery of non-equilibrium grain boundary structures. Highly protective passive films are ascribed to Cr enrichment in the passive film, as evidenced by glow discharge optical emission spectrometry (GD-OES). This Cr enrichment in passive films was reported in UFG and nanostructured Fe–Cr alloys fabricated by mechanical alloying,[145)] and magnetron spattering,[146)] and this was attributed to preferential dissolution of Fe[145,147)] or fast diffusion of Cr at high-density grain boundaries.[146)] By tracer experiment, it was shown that Cr diffusion at grain boundaries in NC Fe processed by SMAT is 4 to 5 times faster than that in CG Fe, and this ultrafast diffusion of Cr in NC Fe is attributed to non-equilibrium grain boundaries.[100)] In our subsequent study using UFG Fe–8, 10, 12%Cr alloys, Fe–12%Cr alloys having both CG and UFG structures exhibited passivity in 3.5% NaCl solutions, and the pitting potential was higher in UFG 12%Cr alloys than in the CG counterpart.[35)] However, more surprisingly, the UFG Fe–8%Cr and 10%Cr alloys exhibited passivity while the CG alloys did not, in the same solution, as shown in Fig. 5.[35)] This was a surprising result because the critical Cr content for self-passivation is established as 11%Cr. As shown in Fig. 6, this passivation appears at an early stage of deformation, but extensive improvement (a higher breaking potential) is seen after 8 passes of ECAP.[36)] This strongly suggests that non-equilibrium grain boundaries may play a critical role in reducing the critical Cr contents for passivity and rendering 8% and 10% Cr alloys *stainless steels*. In addition, this passivation of 8 and 10%Cr steels disappears after post-ECAP annealing at temperatures of 698 to 773 K with little microstructural change (Fig. 7).[36)]

3.7 Effect of area fraction of anode and cathode sites in non-passive environemnts

Although the corrosion resistance of the above simple materials follows Ralston's rule in standard testing solutions, several exceptions have been reported, and they are mostly tested in weak or dilute non-passivating environments. One of the authors reported that the corrosion current of UFG copper by ECAP in Livingston etchant (pH = 1, non-passivation) is lower than that of CG materials in spite of high density defects.[148)] The corrosion current was decreased by the suppression of the cathode curve while the anode curve remained unchanged.[148)] This change may be attributed to kinetics in local cells between grain boundaries and grain interior. In the ultrafine-grained regime, if grain interior regions as cathode sites do not counterbalance the anode sites that become abundant with grain size reduction, the cathode current (cathode slope) is suppressed. Similarly, UFG IF steels processed by ECAP exhibit a lower corrosion rate than CG in weaker solution (0.01 M NaCl), and this goes against Ralston's rule too, whereas the UFG materials exhibited higher corrosion rates in a non-passive stronger solution (1 M NaCl).[149)] An another example which supports this idea was reported for UFG IF steels processed by wire brush for which the corrosion currents of nanograined IF was higher than that of CG materials in a range of solutions consisting of NaCl

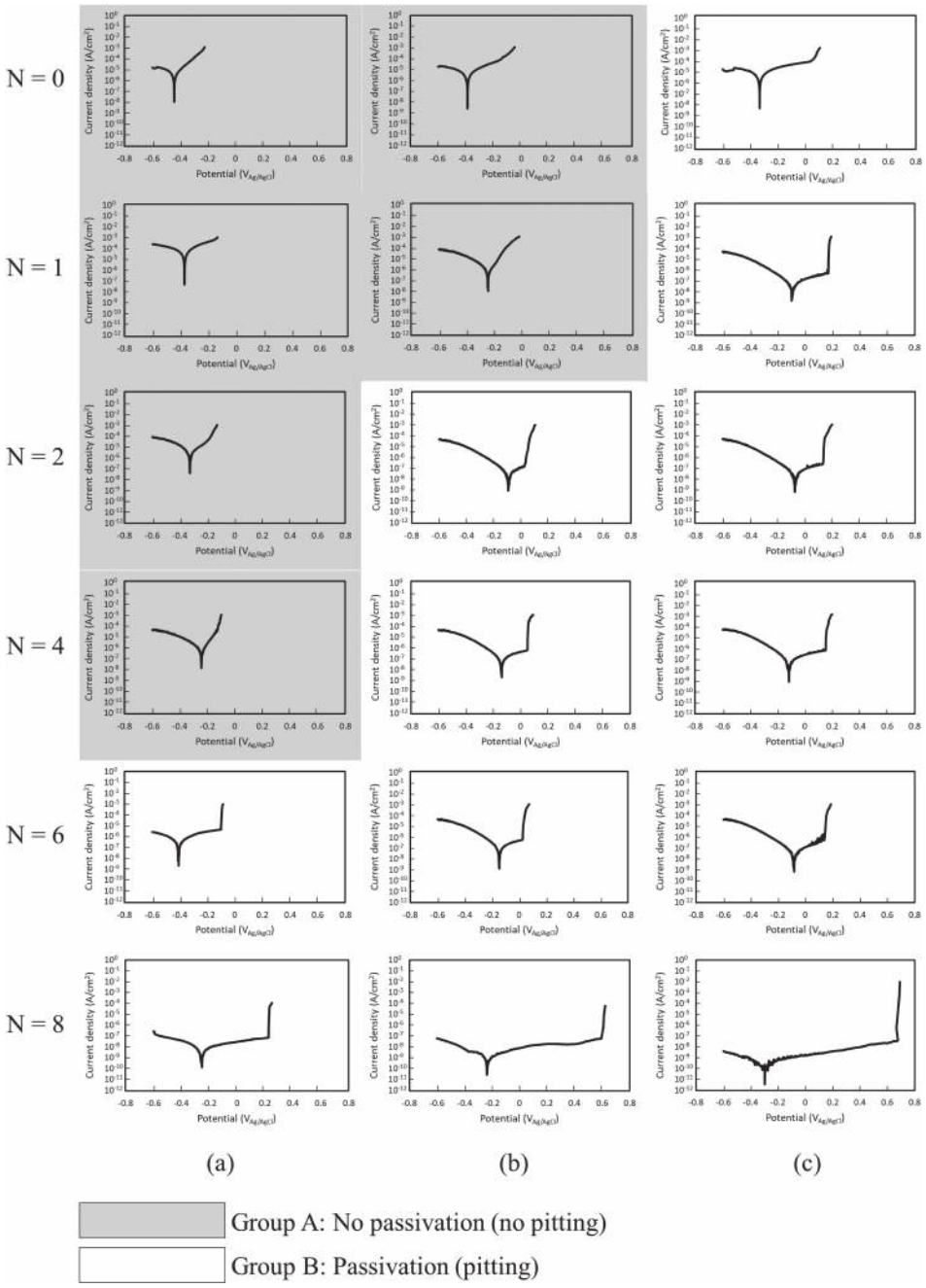

Fig. 6 Dynamic polarization curves of (a) Fe–8%Cr, (b) Fe–10%Cr and (c) Fe–12%Cr steels after each ECAP passes.[36)]

and H_2SO_4.[150)] When the solution is weak with a lower oxidizing power, the corrosion behavior becomes more sensitive to microstructure (grain size and dislocation density) because the solution attacks the materials by more local manner, selecting high energy defects such as grain boundaries and dislocations.[151)] In other words, galvanic cells that are linked to grain boundaries or dislocations become closely spaced at very high strain range and may affect the corrosion kinetics. With such closely spaced galvanic cells, the area fraction of anode sites to cathode sites may also affect corrosion kinetics. According to Uligh,[152)] the maximum corrosion current occurs when the area of anode site is given by $A_c = \beta_c/(\beta_a + \beta_c)$, where β_a and β_c are the Tafel slopes of the anode and cathode reactions, respectively. The grain size reduction will increase the dissolution rate by increasing grain boundaries as anode sites, and this accord with Ralston's rule. However, this increase in corrosion rate is expected to reverse when the grain size becomes extremely small and area of cathode sites is smaller than A_c.

4. General Trends and Corrosion Mechanism of Severely Deformed Metals

4.1 Classification of general trends of corrosion resistance

General trends of corrosion with increasing strain reported in the literature are classified into several types, as shown in Fig. 8. In the figure, corrosion resistance is a symbolic term and specifically indicates pitting potential, polarization resistance, or the inverse of corrosion current from difference

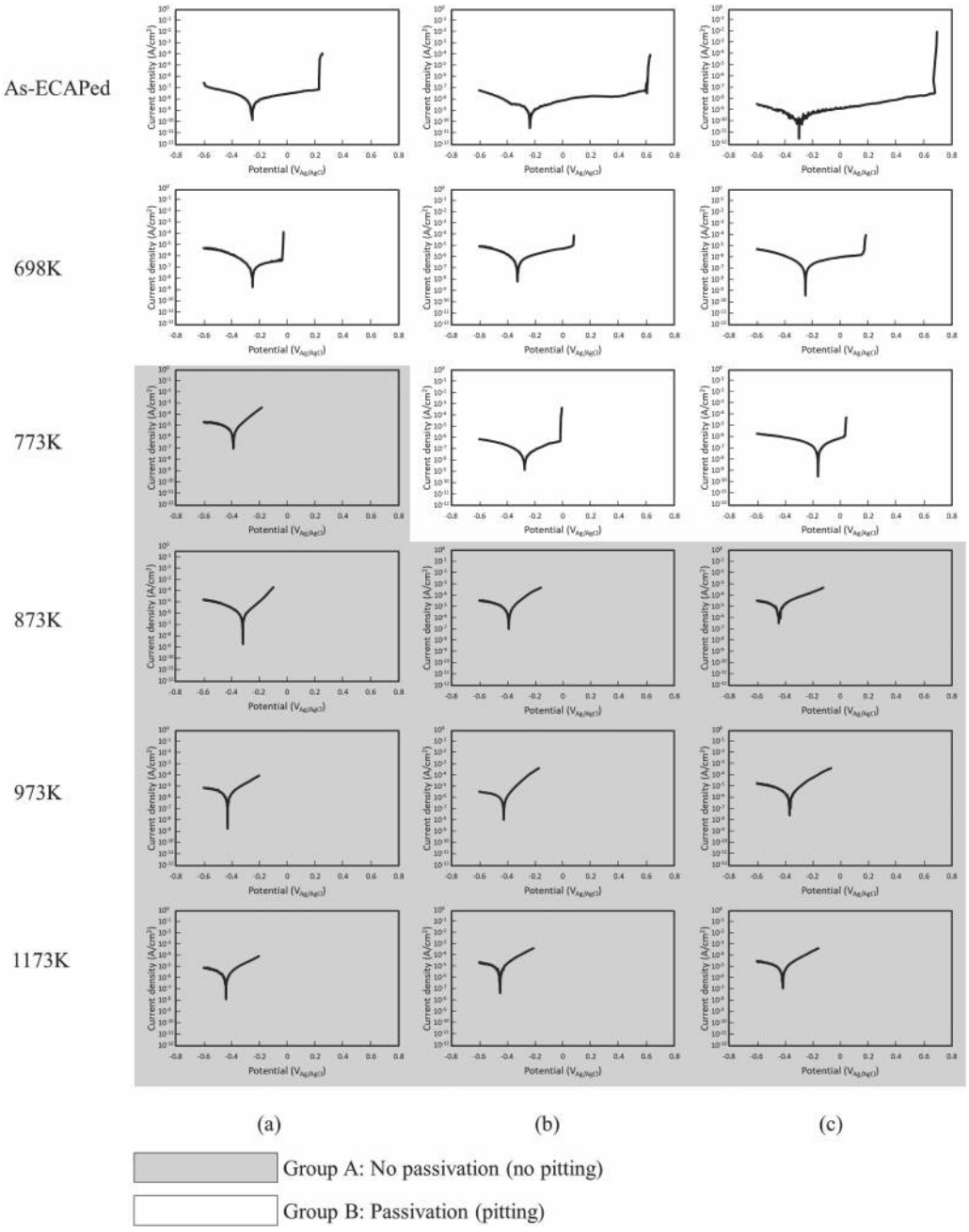

Fig. 7 Dynamic polarization curves of (a) Fe–8%Cr, (b) Fe–10%Cr and (c) Fe–12%Cr steels after post-ECAP annealing at various temperature after ECAP for 8 passes.[37)]

sources.[34,36,39,58,95,107–114)] Type A is the most common trend found in a wide range of materials in passive environments, where corrosion resistance increases with decreasing rate towards saturation. The change seems to be in accord with the stored energy. In type B, the corrosion resistance increases with an abrupt increase at the middle stage, and this may be ascribed to certain microstructural changes or UFG formation. This type of trend is seen in pure copper processed by ARB in NaCl solution[34)] and ECAPed Fe–Cr alloys in NaCl solutions.[29,35)] In type C, the corrosion rate increases with increasing defects density by SPD. In type C′, corrosion resistance decreased in the early stage, but increased with the possible formation of a UFG structure. This type of trend was recognized in pure copper pressed by SSE in Livingston's dislocation etchant.[110)]

4.2 Local potential change at grain boundaries and dislocations

Thermodynamically, the driving force of corrosion is the energy stored by lattice defects, which increases progressively with increasing strain. The relationship between the free energy stored in defects ΔG (J/mol), and resultant change in electrochemical potential ΔE is given by as follows,[151)]

$$\Delta G = -nF\Delta E \tag{1}$$

where n is the change in oxidation number of the metal when it corrodes and F is Faraday' constant. For example, severe cold working of pure copper to induce defects amounting to 160 J/kg, which is equivalent to a dislocation density of $10^{15}\,m^{-2}$, will afford only about 0.1 mV of potential

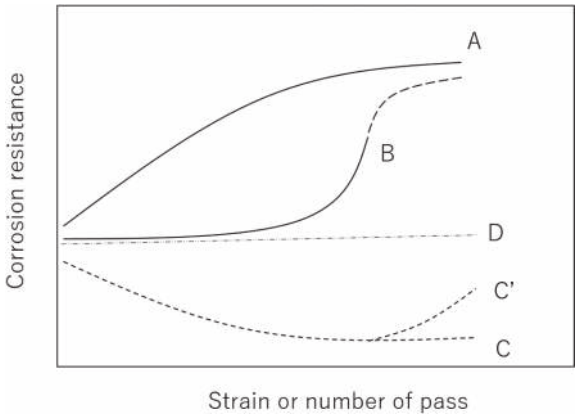

Fig. 8 Classified trends of corrosion resistance with increasing plastic strain. Corrosion resistance represents polarization resistance,[34,95,107,108,111–113] pitting potential,[36,58] the inverse of corrosion current[39,109,110] or weight loss.[110,114] References are type A,[58,109,111–114] type B,[34,36,95] type C,[39,107] type C′[110,113] and type D.[108,113]

difference. Similarly, the potential drop by the transition to UFG of high-density HAGBs from a perfect single crystal is small, and is given by $\Delta E = 3\gamma/D$, where γ is the grain boundary energy of a HAGB (for Cu $\gamma = 0.6\,\mathrm{Jm^{-2}}$), and D is the grain size. For the case $D = 100\,\mathrm{nm}$, $\Delta E = 3 \times 0.6/(100 \times 10^{-9}) = 1.8 \times 10^{7}\,\mathrm{Jm^{-3}}$, which is equivalent to only 0.11 mV. Therefore, the potential change in average-based stored energy is very small by grain reduction and dislocation accumulations even if their density is extremely high. On the other hand, experimental differences in the corrosion potential of CG and UFG pure copper were reported as 30 mV in 3.5% NaCl,[153] and surprisingly reached 100 mV in Livingston's etchant.[148] Because the corrosion potential is determined not only by the electrode potentials, but also by the reaction kinetics which are accelerated by the high local potential of grain boundaries and dislocations, the local stored energy of these single defects must be considered. For example, the grain boundary energy of typical HAGBs in copper is about $600\,\mathrm{mJ/m^2}$. By supposing a grain boundary width of $w = 1\,\mathrm{nm}$, the extra energy per atom in the grain boundary, $\Delta G = E_{\mathrm{gb}}/N = 0.6 \times (3.6 \times 10^{-10})^3/(4 \times 10^{-9}) = 7 \times 10^{-21}\,\mathrm{J}$, where N is the number of atoms belonging to the grain boundary per unit area, and the lattice constant a of copper is $3.6 \times 10^{-10}\,\mathrm{m}$. Therefore, the potential drop at a grain boundary is given by $\Delta E = \Delta G/-ze = -22\,\mathrm{mV}$. This is still lower than the requirement for a galvanic cell, as a minimum potential difference of 30 to 40 mV is generally needed for galvanic corrosion to occur.[151] However, in the presence of a good electrolyte, as little as 15 mV difference in corrosion potential of two sites can form a local cell, and if the difference is 30 mV or greater the anodic materials will definitely corrode sacrificially to protect the neighboring less-active cathodic sites.[151] According to Nazarov,[88] the grain boundary energy in the non-equilibrium state reaches almost double ($1.2\,\mathrm{J/m^2}$) the grain boundary at equilibrium, and in this case, the potential difference amounts to 44 mV which can form a *more rigid* local cell between grain boundaries and the grain interior. Therefore, it may be possible that transient nanoscale galvanic cells may form between grain boundaries and surrounding crystals, and these cells become stronger in non-equilibrium grain boundaries. The possible effect of high-energy non-equilibrium grain boundaries coupled with residual dislocations on corrosion resistance of materials deformed by SPD has been presented for pure copper,[43,144,148] titanium[41,75,139] and stainless steels[29,35,36] by observing change in corrosion behavior by post-SPD annealing. Similarly, the potential difference between a single edge dislocation core and the surrounding potential can be estimated from the dislocation core energy $W_{\mathrm{d}} = \mu b^3/4\pi(1-\upsilon)$ per length of b, where μ is the shear modulus, b is the Burgers vector, and υ is Poisson ratio.[45] If one can assume the core radius to be $2b$, then $W_{\mathrm{d}} = 7.0 \times 10^{-20}\,\mathrm{J}$, which corresponds to the local potential drop reaching 63 mV. Thus, galvanic cells between single dislocations and the surrounding matrix are also possible. Indeed, local potential drops at individual defects were reported in experimental works using Kelvin probes, which exhibited local drops in the electron work function (EWF) reaching 60 to 80 mV in Cu and Al,[154] and 0.1 V in nanograined 304 steels.[47] EWF is directly correlated with the corrosion potential,[155] and the significance of this work is to demonstrate that different levels of electron activity are maintained at the grain boundaries and grain interior and are not *averaged* even in nanocrystalline materials. In another approach using high-angle-annular-dark-field (HAADF)-TEM, Zhou *et al.* estimated the local potential drop at a single dislocation core to be almost 100 mV.[44] In in situ observations by EC-STM, corroded topographic features resulting from nanoscale local dissolution or local passivation at a single grain boundary were observed.[49–51] It was shown that random grain boundaries develop thicker passivation than coherent grain boundaries in microcrystalline copper.[156] In a more direct approach, nanoscale galvanic cells were observed in in situ mode using OL-EPM.[54]

4.3 Effect of dense defects configuration on dissolution

Based on the above consideration, local potential drops and the resulting surface states after corrosion in non-passivating and passivating environments are shown schematically in Fig. 9, with corresponding dislocations and grain boundaries in each SPD stage shown in Fig. 1. The initial structure consists of recrystallized grains with no dislocations inside them. Thus, the potential is uniform with local drops at grain boundaries. In the stage 2, there are many small potential drops at dislocation cores and grain boundaries, and average potential decreases according to the total stored energy. In stage 3 where an ideal UFG structure is formed, potential drops are seen only at grain boundaries, but they become deeper because of higher grain boundary energy. The overall potential inside the grains rises back to the initial level because dislocations are integrated into the grain boundaries. When the UFG structure is recovered by post-SPD annealing with little grain growth (far right), potential drops become shallower by transition back to equilibrium grain boundaries. Accordingly, corroded surfaces are altered according to the above potential distribution and oxidizing power of the solution (level of equilibrium potential of cathode reaction, E_{c}, such as $2\mathrm{H^+} + 2\mathrm{e^-} \rightarrow \mathrm{H_2}$). Ideally, if E_{c} is higher than both $E_{\mathrm{a,g}}$, the potential of the grains, and $E_{\mathrm{a,gb}}$, the potential inside the grains as in the aggressive case, general corrosion

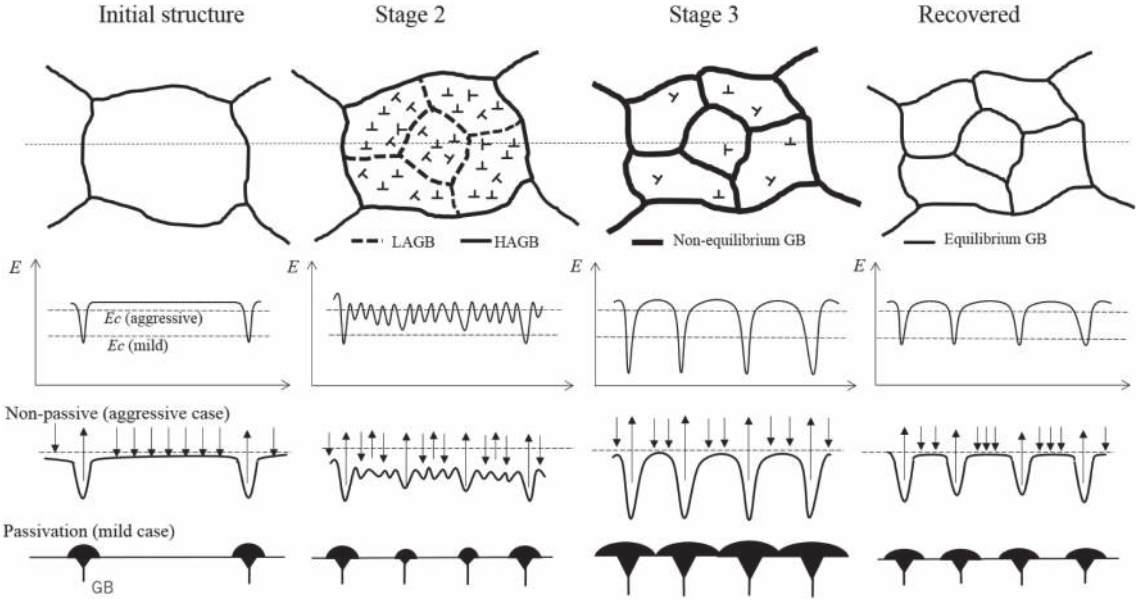

Fig. 9 Schematic diagram showing potential distribution of anodic (metal oxidation) reaction corresponding microstructures (above), corroded surface in non-passivating in relatively aggressive solution (high E_c), and passivation in mild solutions (low E_c) at various stages of SPD shown Fig. 1. E_c is equilibrium potential of cathodic (reduction) reaction.

may occur. In this case, corrosion kinetics either for dissolution or passivation is determined by overall stored energy level. When E_c is between $E_{a,g}$ and $E_{a,gb}$ as in the mild case in Fig. 9, then corrosion becomes selective and limited to defects with a potential lower than E_c.[151] The corrosion rate becomes sensitive to microstructural evolution, and becomes higher or slower with UFG formation depending on E_c level. This consideration is purely based on thermodynamics, the purpose is to interpret the overall trend as a response to structural changes by SPD and post-SPD annealing. For a more thorough discussion of the local corrosion rate, a kinetic mechanism taking the local structure into consideration must be considered.

4.4 Pseudo-uniform corrosion of UFG materials

In a UFG structure, the formation of closely spaced cells of anodic-cathodic reactions with a very high fraction of grain boundaries in the microstructure is likely to make the corroded surface uniform as in general corrosion. In a strict sense, general or uniform corrosion proceeds by forming corrosion cells between anode and cathode sites that are not spatially separated and not fixed at the surface. As a result, the corroded surface is uniform with no intergranular grooves and pitting. In the other extreme, local corrosion such as intergranular corrosion proceeds by forming fixed galvanic cells with separate anode and cathode sites at grain boundaries and grain interior. The degree of localization of anodic dissolution is determined by the electrode potential of dislocations and grain boundaries, and the oxidizing power of the solution.[151] In the present case, anode and cathode sites are linked to lattice defects, but may be transient because if anodic dissolution was confined to a dislocation, it would form a hole along the dislocation line, and it is not probable. The present type of corrosion should be distinguished from the classic general corrosion, and can be considered as *pseudo-uniform* or *pseudo-general* corrosion.

In the UFG regime, the formation of closely spaced cells of anodic-cathodic reactions with a very high fraction of grain boundaries in the microstructure is likely to reduce corrosion in two ways: (1) accelerating the passivation kinetics in highly oxidizing environments, and (2) reducing the intensity of local cell between grain boundaries and grain interior in weak or dilute solution by suppressing cathodic reaction due to smaller area of grains.

5. Conclusions

In corrosion study of severely deformed materials, in which the microstructures become fragmented into ultrafine-grained structures with more or less residual dislocations, grain size has been regarded as the most dominant metallurgical varialbe, and a general universal law involving grain size was pursued. Fortunately, it seems that this notion may be applicable to pure aluminum and pure magnesium, and to other materials of high SFE and low melting temperature in which dynamic recovery or recrystallization occurs relatively easily during SPD and form grain boundaries with few residual dislocations. However, as shown by the systematic investigation of the effect of increasing plastic strain and post-SPD annealing on the corrosion behavior of copper, titanium and steels in which dynamic recovery is rather difficult during SPD, the *side effect* of UFG structures on corrosion is found to be significant due to closely spaced lattice defects. Corrosion behavior was difficult for us to understand in terms of grain size only. In this review, this *side effect* of SPD by non-equilibrium grain boundaries and dislocations is highlighted in stainless steels, which exhibited a very high resistance to corrosion by forming a protective passive film due to very reactive grain boundaries. More generally, the effect of structures and the configuration of grain boundaries and dislocations becomes stronger in UFG structures due to

closely spaced local cells formed by these lattice defects. The local potential distribution due to a single lattice defects can explain the overall tendency to dissolution or passivation in accordance with microstructural development. However, for a more thorough discussion on the effect of configuration of lattice defects on corrosion kinetics that govern the macroscopic corrosion rate, in situ observation of the transient corrosion current at a single-defect scale is needed.

REFERENCES

1) Z.A. Foroulis and H.H. Uhlig: J. Electrochem. Soc. **111** (1964) 522–528.
2) F. Cao, Z. Shi, G.-L. Song, M. Liu, M.S. Dargusch and A. Atrens: Corros. Sci. **90** (2015) 176–191.
3) J. Chen, Q. Xiao, Z. Lu, X. Ru, G. Han, Y. Tian and T. Shoji: Int. J. Electrochem. Sci. **11** (2016) 1395–1415.
4) M. Sahal, J. Creus, R. Sabot and X. Feaugas: Scr. Mater. **51** (2004) 869–873.
5) M. Sahal, J. Creus, R. Sabot and X. Feaugas: Acta Mater. **54** (2006) 2157–2167.
6) R. Singh, B. Ravikumar, A. Kumar, P.K. Dey and I. Chattoraj: Metall. Mater. Trans. A **34** (2003) 2441–2447.
7) J.J. Harwood: Corrosion **6** (1950) 290–307.
8) V.M. Segal, V.I. Reznikov, A.E. Drobyshevskiy and A.E. Kopylov: Russ. Metall. **1** (1981) 99–105.
9) P.W. Bridgman: Phys. Rev. **48** (1935) 825–847.
10) Y. Saito, H. Utsunomiya, N. Tsuji and T. Sakai: Acta Mater. **47** (1999) 579–583.
11) E.A. El-Danaf: Mater. Sci. Eng. A **487** (2008) 189–200.
12) F. Dalla Torre, R. Lapovok, J. Sandlin, P.F. Thomson, C.H.J. Davies and E.V. Pereloma: Acta Mater. **52** (2004) 4819–4832.
13) D. Orlov, N. Kamikawa and N. Tsuji: Philos. Mag. **92** (2012) 2329–2350.
14) B. Jóni, V. Gonda, B. Verö and T. Ungár: IOP Conf. Series Mater. Sci. Eng. **63** (2014) 012136.
15) Y. Miyajima, S.-Y. Komatsu, M. Mitsuhara, S. Hata, H. Nakashima and N. Tsuji: Philos. Mag. **90** (2010) 4475–4488.
16) O.F. Higuera-Cobos and J.M. Cabrera: Mater. Sci. Eng. A **571** (2013) 103–114.
17) A. Mishra, B.K. Kad, F. Gregori and M.A. Meyers: Acta Mater. **55** (2007) 13–28.
18) N. Lugo, N. Llorca, J.M. Cabrera and Z. Horita: Mater. Sci. Eng. A **477** (2008) 366–371.
19) K. Edalati, J.M. Cubero-Sesin, A. Alhamidi, I.F. Mohamed and Z. Horita: Mater. Sci. Eng. A **613** (2014) 103–110.
20) H. Miyamoto: Mater. Trans. **57** (2016) 559–572.
21) K.D. Ralston and N. Birbilis: Corrosion **66** (2010) 075005.
22) G.R. Argade, S.K. Panigrahi and R.S. Mishra: Corros. Sci. **58** (2012) 145–151.
23) N.P. Gurao, G. Manivasagam, P. Govindaraj, R. Asokamani and S. Suwas: Metall. Mater. Trans. A **44** (2013) 5602–5610.
24) C. op't Hoog, N. Birbilis and Y. Estrin: Adv. Eng. Mater. **10** (2008) 579–582.
25) K.D. Ralston, N. Birbilis and C.H.J. Davies: Scr. Mater. **63** (2010) 1201–1204.
26) K.D. Ralston, J.G. Brunner, S. Virtanen and N. Birbilis: Corrosion **67** (2011) 105001–105010.
27) K.D. Ralston, D. Fabijanic and N. Birbilis: Electrochim. Acta **56** (2011) 1729–1736.
28) K.D. Ralston, G. Williams and N. Birbilis: Corrosion **68** (2012) 507–517.
29) M. Rifai, H. Miyamoto and H. Fujiwara: Int. J. Corr. **2015** (2015) 386865.
30) M.W. Grabski: J. Phys. **C4-46** (1985) C4-567.
31) R.Z. Valiev, V.Y. Gertsman and O.A. Kaibyshev: Phys. Status Solidi A **97** (1986) 11–56.
32) A.A. Nazarov: Lett. Mater. **8** (2018) 372–381.
33) D.G. Morris and M.A. Muñoz-Morris: Acta Mater. **50** (2002) 4047–4060.
34) A. Fattah-alhosseini and O. Imantalab: J. Alloys Compd. **632** (2015) 48–52.
35) M. Rifai, M. Yuasa and H. Miyamoto: Metals **8** (2018) 149.
36) M. Rifai, M. Yuasa and H. Miyamoto: Int. J. Corr. **2018** (2018) 4853175.
37) H.S. Kim, S.J. Yoo, J.W. Ahn, D.H. Kim and W.J. Kim: Mater. Sci. Eng. A **528** (2011) 8479–8485.
38) H.S. Kim and W.J. Kim: Corros. Sci. **75** (2013) 228–238.
39) D. Song, A. Ma, J. Jiang, P. Lin, D. Yang and J. Fan: Corros. Sci. **52** (2010) 481–490.
40) X.Y. Wang and D.Y. Li: Electrochim. Acta **47** (2002) 3939–3947.
41) H.S. Kim and W.J. Kim: Corros. Sci. **89** (2014) 331–337.
42) H.Y. Choi and W.J. Kim: J. Mech. Behav. Biomed. Mater. **51** (2015) 291–301.
43) D. Yang, Y. Dong, H. Chang, I. Alexandrov, F. Li, J. Wang and Z. Dan: Mater. Corr. **69** (2018) 1455–1461.
44) Y.T. Zhou, Y.J. Wang, S.J. Zheng, B. Zhang and X.L. Ma: Philos. Mag. **95** (2015) 2365–2375.
45) E.M. Gutman: *Mechanochemistry of Materials*, (Cambridge International Science Publishing, United Kingdom, 1998).
46) D.Y. Li: MRS Proc. **887** (2005) 0887-Q05-03.
47) L. Jinlong and L. Hongyun: J. Nucl. Mater. **452** (2014) 469–473.
48) D.B. Blücher, J.-E. Svensson, L.-G. Johansson, M. Rohwerder and M. Stratmann: J. Electrochem. Soc. **151** (2004) B621–B626.
49) E. Martinez-Lombardia, L. Lapeire, V. Maurice, I. De Graeve, K. Verbeken, L.H. Klein, L.A.I. Kestens, P. Marcus and H. Terryn: Electrochem. Commun. **41** (2014) 1–4.
50) H. Chen, V. Maurice, L.H. Klein, L. Lapeire, K. Verbeken, H. Terryn and P. Marcus: J. Solid State Electrochem. **19** (2015) 3501–3509.
51) M. Bettayeb, V. Maurice, L.H. Klein, L. Lapeire, K. Verbeken and P. Marcus: J. Electrochem. Soc. **165** (2018) C835–C841.
52) B. Zhang, J. Wang, B. Wu, E.E. Oguzie, K. Luo and X.L. Ma: Sci. Rep. **6** (2016) 39525.
53) N. Kobayashi, H. Asakawa and T. Fukuma: J. Appl. Phys. **110** (2011) 044315.
54) K. Honbo, S. Ogata, T. Kitagawa, T. Okamoto, N. Kobayashi, I. Sugimoto, S. Shima, A. Fukunaga, C. Takatoh and T. Fukuma: ACS Nano **10** (2016) 2575–2583.
55) M. Laleh and F. Kargar: Mater. Lett. **65** (2011) 1935–1937.
56) M. Laleh and F. Kargar: J. Alloys Compd. **509** (2011) 9150–9156.
57) E. Akiyama, Z. Zhang, Y. Watanabe and K. Tsuzaki: J. Solid State Electrochem. **13** (2009) 277–282.
58) M.-K. Chung, Y.-S. Choi, J.-G. Kim, Y.-M. Kim and J.-C. Lee: Mater. Sci. Eng. A **366** (2004) 282–291.
59) I.J. Son, H. Nakano, S. Oue, S. Kobayashi, H. Fukushima and Z. Horita: Mater. Trans. **47** (2006) 1163–1169.
60) I.J. Son, H. Nakano, S. Oue, S. Kobayashi, H. Fukushima and Z. Horita: Mater. Trans. **48** (2007) 21–28.
61) M. Hockauf, L.W. Meyer, D. Nickel, G. Alisch, T. Lampke, B. Wielage and L. Kruger: J. Mater. Sci. **43** (2008) 7409–7417.
62) I.J. Son, H. Nakano, S. Oue, S. Kobayashi, H. Fukushima and Z. Horita: Mater. Trans. **49** (2008) 2648–2655.
63) M. Pisarek, P. Kedzierzawski, M. Janik-Czachor and K.J. Kurzydlowski: Corrosion **64** (2008) 131–137.
64) I.J. Son, H. Nakano, S. Oue, S. Kobayashi, H. Fukushima and Z. Horita: Trans. Nonferrous Met. Soc. China **19** (2009) 904–908.
65) J.H. Gao, S.K. Guan, Z.W. Ren, Y.F. Sun, S.J. Zhu and B. Wang: Mater. Lett. **65** (2011) 691–693.
66) M.F. Naeini, M.H. Shariat and M. Eizadjou: J. Alloys Compd. **509** (2011) 4696–4700.
67) D. Orlov, K.D. Ralston, N. Birbilis and Y. Estrin: Acta Mater. **59** (2011) 6176–6186.
68) D. Song, A.B. Ma, J.H. Jiang, P.H. Lin and J. Shi: Corros. Eng. Sci. Technol. **46** (2011) 505–512.
69) D. Song, A.B. Ma, J.H. Jiang, P.H. Lin, D.H. Yang and J.F. Fan: Corros. Sci. **53** (2011) 362–373.
70) Z.J. Zheng, Y. Gao, Y. Gui and M. Zhu: Corros. Sci. **54** (2012) 60–67.
71) S. Li, Z. Ren, Y. Dong, C. Ye, G. Cheng and H. Cong: J. Electrochem. Soc. **164** (2017) C682–C689.
72) Z. Pu, S. Yang, G.L. Song, O.W. Dillon, Jr., D.A. Puleo and I.S.

Jawahir: Scr. Mater. **65** (2011) 520–523.
73) B.N. Mordyuk, O.P. Karasevskaya, G.I. Prokopenko and N.I. Khripta: Surf. Coat. Tech. **210** (2012) 54–61.
74) B.N. Mordyuk, O.P. Karasevskaya and G.I. Prokopenko: Mater. Sci. Eng. A **559** (2013) 453–461.
75) Y. Gu, A. Ma, J. Jiang, H. Li, D. Song, H. Wu and Y. Yuan: Mater. Charact. **138** (2018) 38–47.
76) H. Garbacz, M. Pisarek and K.J. Kurzydłowski: Biomol. Eng. **24** (2007) 559–563.
77) V. Pandey, J.K. Singh, K. Chattopadhyay, N.C.S. Srinivas and V. Singh: J. Alloys Compd. **723** (2017) 826–840.
78) Y. Cao, S. Ni, X. Liao, M. Song and Y. Zhu: Mater. Sci. Eng. Rep. **133** (2018) 1–59.
79) K. Edalati and Z. Horita: Acta Mater. **59** (2011) 6831–6836.
80) Y. Estrin and A. Vinogradov: Acta Mater. **61** (2013) 782–817.
81) N.R. Tao, Z.B. Wang, W.P. Tong, M.L. Sui, J. Lu and K. Lu: Acta Mater. **50** (2002) 4603–4616.
82) H.J. Maier, P. Gabor, N. Gupta, I. Karaman and M. Haouaoui: Int. J. Fatigue **28** (2006) 243–250.
83) P.-L. Sun, P.-W. Kao and C.-P. Chang: Metall. Mater. Trans. A **35** (2004) 1359–1368.
84) Y. Iwahashi, Z. Horita, M. Nemoto and T.G. Langdon: Acta Metall. Mater. **45** (1997) 4733–4741.
85) P.W.J. Mckenzie, R. Lapovok and Y. Estrin: Acta Mater. **55** (2007) 2985–2993.
86) K. Edalati, D. Akama, A. Nishio, S. Lee, Y. Yonenaga, J.M. Cubero-Sesin and Z. Horita: Acta Mater. **69** (2014) 68–77.
87) P. Xue, B.B. Wang, F.F. Chen, W.G. Wang, B.L. Xiao and Z.Y. Ma: Mater. Charact. **121** (2016) 187–194.
88) A.A. Nazarov, A.E. Romanov and R.Z. Valiev: Scr. Mater. **34** (1996) 729–734.
89) A.A. Nazarov, A.E. Romanov and R.Z. Valiev: Acta Metall. Mater. **41** (1993) 1033–1040.
90) R.Z. Valiev, R.K. Islamgaliev and I.V. Alexandrov: Prog. Mater. Sci. **45** (2000) 103–189.
91) W. Wei, K.X. Wei and Q.B. Du: Mater. Sci. Eng. A **454–455** (2007) 536–541.
92) I.J. Son, H. Nakano, S. Oue, S. Kobayashi, H. Fukushima and Z. Horita: Mater. Trans. **49** (2008) 2656–2663.
93) D. Song, A.B. Ma, J.H. Jiang, P.H. Lin and D.H. Yang: Trans. Nonferrous Met. Soc. China **19** (2009) 1065–1070.
94) X. Wang, M. Nie, C.T. Wang, S.C. Wang and N. Gao: Mater. Des. **83** (2015) 193–202.
95) A. Fattah-alhosseini and S.O. Gashti: J. Mater. Eng. Perform. **24** (2015) 3386–3393.
96) X. Sauvage, G. Wilde, S.V. Divinski, Z. Horita and R.Z. Valiev: Mater. Sci. Eng. A **540** (2012) 1–12.
97) S. Divinski, J. Ribbe, G. Reglitz, Y. Estrin and G. Wilde: J. Appl. Phys. **106** (2009) 063502.
98) S.V. Divinski, G. Reglitz, I.S. Golovin, M. Peterlechner, R. Lapovok, Y. Estrin and G. Wilde: Acta Mater. **82** (2015) 11–21.
99) S.V. Divinski, J. Ribbe, G. Reglitz, Y. Estrin and G. Wilde: J. Appl. Phys. **106** (2009) 063502.
100) Z.B. Wang, N.R. Tao, W.P. Tong, J. Lu and K. Lu: Acta Mater. **51** (2003) 4319–4329.
101) V.Y. Gertsman, R. Birringer, R.Z. Valiev and H. Gleiter: Scr. Metall. Mater. **30** (1994) 229–234.
102) J. Wang, Y. Iwahashi, Z. Horita, M. Furukawa, M. Nemoto, R.Z. Valiev and T.G. Langdon: Acta Metall. Mater. **44** (1996) 2973–2982.
103) L. Priester: Interface Sci. **4** (1997) 205–219.
104) W.Q. Cao, C.F. Gu, E.V. Pereloma and C.H.J. Davies: Mater. Sci. Eng. A **492** (2008) 74–79.
105) Y. Zhang, J.T. Wang, C. Cheng and J. Liu: J. Mater. Sci. **43** (2008) 7326.
106) E. Schafler, G. Steiner, E. Korznikova, M. Kerber and M.J. Zehetbauer: Mater. Sci. Eng. A **410–411** (2005) 169–173.
107) M. Eizadjou, H. Fattahi, A.K. Talachi, H.D. Manesh, K. Janghorban and M.H. Shariat: Corros. Eng. Sci. Technol. **47** (2012) 19–24.
108) O. Jilani, N. Njah and P. Ponthiaux: Corros. Sci. **87** (2014) 259–264.
109) N. Birbilis, K.D. Ralston, S. Virtanen, H.L. Fraser and C.H.J. Davis: Corros. Eng. Sci. Technol. **45** (2010) 224–230.
110) M. Rifai, E. Bagherpour, G. Yamamoto, M. Yuasa and H. Miyamoto: Adv. Mater. Sci. Eng. **2018** (2018) 4254156.
111) H. Maleki-Ghaleh, K. Hajizadeh, E. Aghaie, S. Ghobadi Alamdari, M. Hosseini, M.H. Fathi, K. Ozaltin and K.J. Kurzydlowski: Corrosion **71** (2015) 367–375.
112) D. Gholami, O. Imantalab, M. Naseri, S. Vafaeian and A. Fattah-alhosseini: J. Alloys Compd. **723** (2017) 856–865.
113) L. Zhang, A. Ma, J. Jiang, D. Yang, D. Song and J. Chen: Corros. Sci. **75** (2013) 434–442.
114) M.I. Abd El Aal and M.M. Sadawy: Trans. Nonferrous Met. Soc. China **25** (2015) 3865–3876.
115) M. Nie, C.T. Wang, M. Qu, N. Gao, J.A. Wharton and T.G. Langdon: J. Mater. Sci. **49** (2014) 2824–2831.
116) S. Bagherifard, D.J. Hickey, A.C. de Luca, V.N. Malheiro, A.E. Markaki, M. Guagliano and T.J. Webster: Biomaterials **73** (2015) 185–197.
117) S. Bagherifard, D.J. Hickey, S. Fintová, F. Pastorek, I. Fernandez-Pariente, M. Bandini, T.J. Webster and M. Guagliano: Acta Biomater. **66** (2018) 93–108.
118) C. Liu, H. Zheng, X. Gu, B. Jiang and J. Liang: J. Alloys Compd. **770** (2019) 500–506.
119) T. Wang, J. Yu and B. Dong: Surf. Coat. Tech. **200** (2006) 4777–4781.
120) H.-s. Lee, D.-s. Kim, J.-s. Jung, Y.-s. Pyoun and K. Shin: Corros. Sci. **51** (2009) 2826–2830.
121) B.N. Mordyuk, G.I. Prokopenko, M.A. Vasylyev and M.O. Iefimov: Mater. Sci. Eng. A **458** (2007) 253–261.
122) T. Balusamy, S. Kumar and T.S.N. Sankara Narayanan: Corros. Sci. **52** (2010) 3826–3834.
123) A. Fattah-Alhosseini, F.R. Attarzadeh and M. Vakili-Azghandi: Metall. Mater. Trans. A **48** (2017) 403–411.
124) I. Son, H. Nakano, S. Oue, S. Kobayashi, H. Fukushima and Z. Horita: Int. J. Corr. **2012** (2012) 450854.
125) A. Korchef and A. Kahoul: Int. J. Corr. **2013** (2013) 983261.
126) E.S.M. Sherif, M.S. Soliman, E.A. El-Danaf and A.A. Almajid: Int. J. Electrochem. Sci. **8** (2013) 1103–1116.
127) E.S.M. Sherif, E.A. El-Danaf, M.S. Soliman and A.A. Almajid: Int. J. Electrochem. Sci. **7** (2012) 2846–2859.
128) O. Jilani, N. Njah and P. Ponthiaux: Corros. Sci. **89** (2014) 163–170.
129) Z. Li, S.J. Zhou and N. Huang: Int. J. Miner. Metall. Mater. **22** (2015) 639–647.
130) C.L.P. Silva, A.C. Oliveira, C.G.F. Costa, R.B. Figueiredo, M. de Fátima Leite, M.M. Pereira, V.F.C. Lins and T.G. Langdon: J. Mater. Sci. **52** (2017) 5992–6003.
131) Z. Li, N. Huang, J. Zhao and S.J. Zhou: Mater. Sci. Technol. **29** (2013) 140–147.
132) N. Li, Y.D. Li, Y.X. Li, Y.H. Wu, Y.F. Zheng and Y. Han: Mater. Sci. Eng. C **35** (2014) 314–321.
133) E. Mostaed, M. Vedani, M. Hashempour and M. Bestetti: Biomatter **4** (2014) e28283.
134) A. Balyanov, J. Kutnyakova, N.A. Amirkhanova, V. Stolyarov, R.Z. Valiev, X.Z. Liao, Y.H. Zhao, Y.B. Jiang, H.F. Xu, T.C. Lowe and Y.T. Zhu: Scr. Mater. **51** (2004) 225–229.
135) A. Balakrishnan, B.C. Lee, T.N. Kim and B.B. Panigrahi: Trends Biomater. Artif. Organs **22** (2008) 58–64.
136) M. Hoseini, A. Shahryari, S. Omanovic and J.A. Szpunar: Corros. Sci. **51** (2009) 3064–3067.
137) H. Maleki-Ghaleh, K. Hajizadeh, A. Hadjizadeh, M.S. Shakeri, S. Ghobadi Alamdari, S. Masoudfar, E. Aghaie, M. Javidi, J. Zdunek and K.J. Kurzydlowski: Mater. Sci. Eng. C **39** (2014) 299–304.
138) E. Matykina, R. Arrabal, R.Z. Valiev, J.M. Molina-Aldareguia, P. Belov and I. Sabirov: Electrochim. Acta **176** (2015) 1221–1232.
139) A. Sotniczuk, D. Kuczyńska-Zemła, A. Królikowski and H. Garbacz: Corros. Sci. **147** (2019) 342–349.
140) Z. Horita, B.C. Smith, M. Nemoto, R. Valiev and T.G. Langdon: J. Mater. Res. **13** (1998) 446–450.
141) V.Y. Gertsman, R. Birringer and R.Z. Valiev: Phys. Status Solidi A **149** (1995) 243–252.
142) M.J. Zehetbauer, H.P. Stüwe, A. Vorhauer, E. Schafler and J. Kohout: Adv. Eng. Mater. **5** (2003) 330–337.
143) F. Salimyanfard, M. Reza Toroghinejad, F. Ashrafizadeh and M. Jafari: Mater. Sci. Eng. A **528** (2011) 5348–5355.

144) A. Vinogradov, T. Mimaki, S. Hashimoto and R.Z. Valiev: Scr. Mater. **41** (1999) 319–326.
145) R. Gupta, R.K. Singh Raman and C.C. Koch: J. Mater. Sci. **47** (2012) 6118–6124.
146) C. Pan, L. Liu, Z. Bin and F. Wang: J. Electrochem. Soc. **159** (2012) C453–C460.
147) R.K. Gupta, R.K. Singh Raman, C.C. Koch and B.S. Murty: Int. J. Electrochem. Sci. **8** (2013) 6791–6806.
148) H. Miyamoto, K. Harada, T. Mimaki, A. Vinogradov and S. Hashimoto: Corros. Sci. **50** (2008) 1215–1220.
149) B. Hadzima, M. Janeček, Y. Estrin and H.S. Kim: Mater. Sci. Eng. A **462** (2007) 243–247.
150) K. Dehghani, M. Hosseini and A. Nekahi: Int. J. Mater. Res. **104** (2013) 999–1006.
151) J.N. Noel: *ASM Handbook 13A Corrosion: Fundamentals, Testing, and Protection*, ed. by S.D. Cramer and B.S.J. Covino, (ASM international, Materials Park, Ohio, 2003) p. 258.
152) H.H. Uhlig and R.W. Revie: *Corrosion and Corrosion Control; Introduction to Corrosion Science and Engineering*, (John Wiley & Sons, Hoboken, 1985).
153) R.J. Hellmig, M. Janeček, B. Hadzima, O.V. Gendelman, M. Shapiro, X. Molodova, A. Springer and Y. Estrin: Mater. Trans. **49** (2008) 31–37.
154) W. Li and D.Y. Li: Surf. Rev. Lett. **11** (2004) 173–178.
155) M. Stratmann, H. Streckel, K.T. Kim and S. Crockett: Corros. Sci. **30** (1990) 715–734.
156) H. Chen, M. Bettayeb, V. Maurice, L.H. Klein, L. Lapeire, K. Verbeken, H. Terryn and P. Marcus: Corros. Sci. **111** (2016) 659–666.